Anharmonicity and Phase Diagram of Magnesium Oxide in the Megabar Regime

François Soubiran[1,2,3] and Burkhard Militzer[1,4]

[1]*Department of Earth and Planetary Science, University of California, Berkeley, California 94720, USA*
[2]*École Normale Supérieure de Lyon, Université Lyon 1, Laboratoire de Géologie de Lyon,
CNRS UMR 5276, 69364 Lyon Cedex 07, France*
[3]*CEA DAM-DIF, 91297 Arpajon, France*
[4]*Department of Astronomy, University of California, Berkeley, California 94720, USA*

With density functional molecular dynamics simulations, we computed the phase diagram of MgO from 50 to 2000 GPa up to 20 000 K. Via thermodynamic integration (TDI), we derive the Gibbs free energies of the B1, B2, and liquid phases and determine their phase boundaries. With TDI and a pseudo-quasi-harmonic approach, we show that anharmonic effects are important and stabilize the B1 phase in particular. As a result, the B1-B2 transition boundary in the pressure-temperature plane exhibits a steep slope. We predict the B1-B2-liquid triple point to occur at approximately $T = 10000$ K and $P = 370$ GPa, which is higher in pressure than was inferred with quasiharmonic methods alone. We predict the principal shock Hugoniot curve to enter the B2 phase stability domain but only over a very small range of parameters. This may render it difficult to observe this phase with shock experiments because of kinetic effects.

DOI: 10.1103/PhysRevLett.125.175701

While early ground-based exoplanet search campaigns detected only giant exoplanets [1], the following surveys conducted with the Kepler [2] and CoRoT [3] spacecrafts determined that most exoplanets have between one and four Earth radii and thus rocky and icy interiors are most common. The determination of the equations of state (EOS), phase diagrams, and physical properties of the materials that are likely to be present in the interiors of exoplanets is a cornerstone in characterization and modeling of these newly discovered and unexpectedly diverse objects. Magnesium oxide is one of the most abundant materials in Earth [4], and is assumed to be a major component in Super-Earths as well [5,6]. MgO is also likely present in the core of Mini-Neptunes and icy giants [7,8]. Even in the interior of gas giant planets, MgO may be present as a constituent in a partially dissolved core [9–11]. In order to describe these different planets, a careful characterization of MgO on a wide range of pressure-temperature conditions is needed. For instance, in Earth, the core-mantle boundary is at 135 GPa while in the gas giant planets, the typical pressure values at boundary between the rocky cores and the gas envelope reaches several TPa. The corresponding temperature may be as high as 20 000 to 30 000 K [12].

In Earth's mantle, MgO occurs in an NaCl-type (B1) structure [13,14]. At approximately 600 GPa, a transformation to a CsCl (B2) structure has been observed experimentally [15]. However, the exact pressure-temperature conditions of this phase transition are still highly debated. At 0 K, *ab initio* calculations based on lattice dynamics place the transition around 500 GPa [16] while quantum Monte Carlo simulations predict it at approximately 600 GPa [17]. At finite temperature, most *ab initio* lattice dynamics calculations predict a negative Clapeyron slope but the steepness of the slope varies significantly from one calculation to another [18–23].

The melting curves of the B1 and B2 phases are not yet well determined. Various numerical methods predicted a melting temperature that differed by up to 2000 K in the multimegabar regime [19–22,24]. A direct consequence of this uncertainty is a significant variability in the location of the triple point. It has been predicted to occur as low as 250 GPa and 8000 K with the quasiharmonic approximation for the solids [25] while calculations that relied on molecular dynamics predicted higher values up to 364 GPa and 12 000 K [19]. The differences between these two types of predictions provide some indication that anharmonic effects must be particularly important for the determination of the MgO triple point.

Magnesium oxide has also been studied experimentally, especially along the principal shock Hugoniot curve using single and decaying shock waves [13,20,26–28]. Both decaying shock experiments [26,27] exhibited a region where the shock temperature increased significantly with decreasing pressure. However, the pressure-temperature conditions, where this drop was observed, were not in perfect agreement. Thus, in one study it has been attributed to the B1-B2 phase transformation and to shock melting in the other. The inconsistency in these findings and their interpretation underlines the need for additional investigations with complementary experimental and computational methods.

In this Letter we report results from density functional molecular dynamics (MD) simulations in combination with thermodynamic integration in order to derive the Gibbs free energy with high precision. We constrain the location of the triple point and derive the stability fields of B1, B2, and liquid phase up to 2000 GPa. All phases are treated consistently with the same method. Since our Gibbs free energy calculations rely on MD, anharmonic effects are naturally included. By comparing with the quasiharmonic approximation, we demonstrate that the anharmonicity is much more important in the B1 than in the B2 phase. Contrary to quasiharmonic predictions, we find a much steeper Clapeyron slope for the B1-B2 phase transition. Finally we derive the shock Hugoniot curve. Consistent with earlier work, we predict this curve to first encounter the B1-B2 transition and then the melting transition, although detecting these transitions in experiments may be hindered by kinetic effects.

We performed our MD simulations with the Vienna *ab initio* simulation package (VASP) [29]. We kept the density and temperature constant, employing a Nosé thermostat [30,31]. The simulation cell contained 64 atoms for the liquid and B1 phases, and 250 for the B2. We confirmed that the residual finite-size effects were negligible for the purpose of this study. When we increased the number of atoms we only observed deviations less or equal to 0.5% in pressure and 0.1 mHa per atom in the energy. We even ensured that the phase boundary of the B1-B2 transition was converged with these cell sizes. We used a time step of 0.5 fs for a total duration of at least 2 ps for the large cells and 10 ps for the small ones. These are only simulation times used for averaging. We ensured that the cells were fully equilibrated before performing the averages. The density functional theory (DFT) calculation was performed using the finite temperature [32] Kohn-Sham scheme [33]. We employed the Perdew, Burke, and Ernzerhof (PBE) functional [34]. We used projector augmented wave (PAW) pseudopotentials [35] with $1s^2$ frozen cores. We used only the Γ point to sample the Brillouin zone since it yielded results that were consistent with those from denser K-point grids. We set the energy cutoff to 1200 eV. The number of bands was adjusted to capture the full spectrum of partially occupied states accurately.

The Helmholtz free energy was computed using the thermodynamic integration (TDI) technique [36–44]. For given density, temperature, and phase, we smoothly switched between an ensemble governed by the DFT potential U_{DFT} to a classical potential U_{cl} of known free energy F_{cl}. For the liquid phase, we used a set of non-bonding pair potentials fitted to forces derived from MD simulations at high temperature in order to include a sufficient number of strong collisions [43]. As described in Ref. [42], for the solid phases, we combined classical pair potentials with Einstein potentials that were fitted to solid simulations of the B1 and B2 phases. We chose to not apply a center-of-mass correction [45] since it appears that the usual Frenkel *et al.* correction is overestimating the actual necessary correction (see Supplemental Material [46]). More recent derivations of the center-of-mass correction [47] have a negligible impact on the phase diagram even for 64 atoms.

We also performed phonon calculations in order to characterize the importance of anharmonic effects. First we extracted the phonon eigenfrequencies and eigenvectors for the B1 and B2 phases using the finite displacement method at $T = 0$ K. We employed the same *ab initio* parameters as in our MD simulations. The eigenfrequencies allowed us to compute the Helmholtz free energy at finite temperature in the quasiharmonic approximation [48].

We studied the temperature dependence of the phonon frequencies using our MD trajectories. For a given configuration, we projected the MD velocities on every eigenvector in a set of phonon modes obtained for the same density at $T = 0$ K. By repeating this projection for many configurations along a trajectory, we computed the autocorrelation function of the mode-projected velocities and extracted their characteristic frequency by Fourier transform [49]. This projection quasiharmonic approach (PQHA) allows us to obtain at finite temperature a corrected set of eigenfrequencies that captures some but not all the anharmonic effects in the system. Using these updated frequencies, we derived corrected free energies.

To determine the relative stability of the different phases, we computed the Gibbs free energy $G = F + PV$ for every density-temperature point. In our QHA calculations, we used the QHA free energies but the pressure term that we have derived from DFT-MD. While not entirely consistent, it allows us to compare more directly with the TDI results and determine how much the B1-B2 phase boundary is shifted by anharmonic effects. For each phase and temperature, we used a cubic spline interpolation of the Gibbs free energy as a function of the pressure. When compared with other interpolation schemes we found very similar results. For given P and T, we identified the phase with the lowest Gibbs free energy to be the most stable. A phase transition occurs where Gibbs free energies are equal. The uncertainties shown in our figures are the propagated 1σ error bars. For instance, to derive the error bars in Fig. 1 we proceeded in two steps. First, for each simulation we used a blocking average method [50] to determine the statistical uncertainty on the pressure and the free energy. Second, as we locate the intersection of two Gibbs free energy interpolations to determine the phase boundaries, we also used finite differences to determine the derivative of the transition pressure with respect to each interpolation parameters. Combining these derivatives with the uncertainties in an error propagation formula we obtained the error bars plotted on Fig. 1.

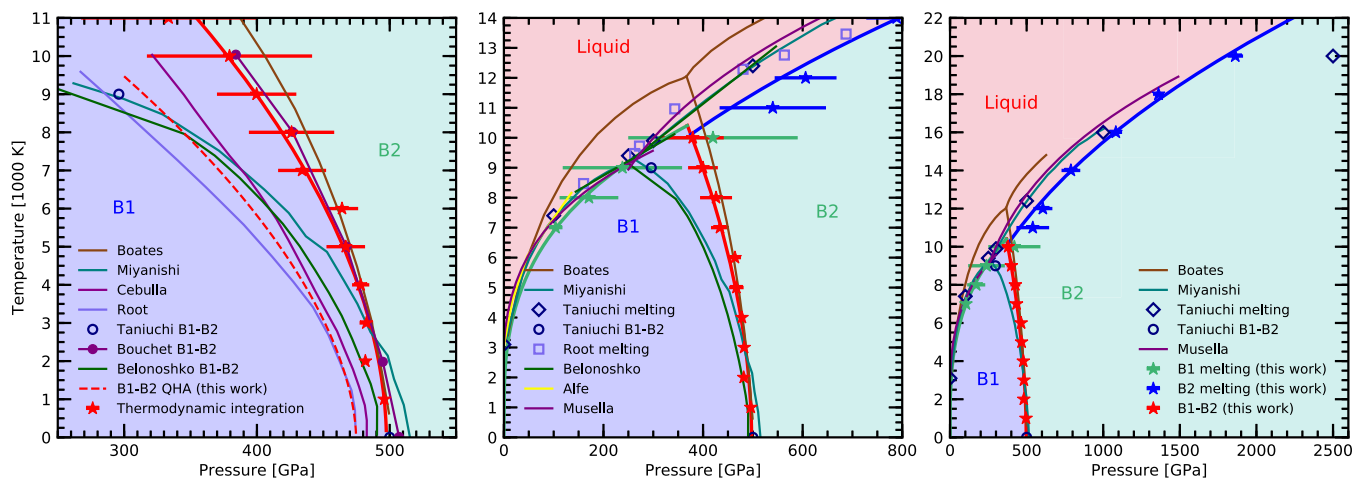Fig. 1 shows our phase diagram. We derived the MgO melting curve between 7000 and 20 000 K, and between 80

FIG. 1.   MgO phase diagram. Left: Low temperature part of the B1-B2 phase transitions. Our TDI results (stars) are compared with Refs. [51,18–25]. Middle: Comparison of our B1-B2-liquid phase boundaries with the literature. Right: Comparison of the melting line up to 2000 GPa.

and 1800 GPa, which includes the B1 and B2 branches at lower and higher pressures. Our B1 melting line is in good agreement with predictions by Miyanishi *et al.* [21] and Taniuchi *et al.* [22] but slightly lower than that of Boates and Bonev [19]. We also note that our phase diagram is consistent with the experimental results from Fat'yanov *et al.* [28] who found the B1 MgO phase to be stable at 248 GPa and 9100 K. For the B2 melting line we find a globally lower melting temperature, except at very high pressure, for which we find a higher melting temperature than Taniuchi *et al.* For the B1 and B2 phases, we fitted the melting line with a *P-T* power law as a guide for the eye since the error bars near the triple point are fairly large.

The most striking feature in our MgO phase diagram is the location of the B1-B2 phase transition. With the TDI method, we obtained among the steepest slope in the pressure-temperature plane. As a result we obtain a fairly high pressure for the triple point. By looking at the intersection of the fitted melting lines with the fitted B1-B2 boundary, we estimate the triple point to lie at approximately 10 000 K and 370 GPa. These results are compatible with the sole experiment that directly observed the MgO B2 phase in ramp compression and x-ray diffraction [15] but in contrast to other numerical results that were reported in the literature [16,18,20,21], all exhibiting a negative but shallower Clapeyron slope and much lower pressure and temperature for the triple point. However, our predictions for the B1-B2 phase transition are in very good agreement with Refs. [19,23] who included strong anharmonicity in their calculations.

To characterize the anharmonic effects, we performed a systematic phonon study of the B1 and B2 phases. In Fig. 2, we compared the phonon spectra that were derived from the QHA at zero temperature with the spectra obtained from PQHA at finite temperature. At $T = 0$ K, on average, the phonon frequencies are lower in the B2 than in the B1

phase. With rising temperature, the average frequency of the B2 phase increases very slightly while a significant softening of the vibrational modes is seen for the B1 phase. This provides a first indication that anharmonic contributions affect both phases very differently.

In Fig. 3, we compared the Helmholtz free energy derived with TDI, QHA, and PQHA. In the B2 phase, we retrieve a very similar free energy with QHA and PQHA, as expected, based on the very similar average frequencies (see Fig. 2). The properties of the phonon in the B2 phase are thus nearly temperature independent. The TDI
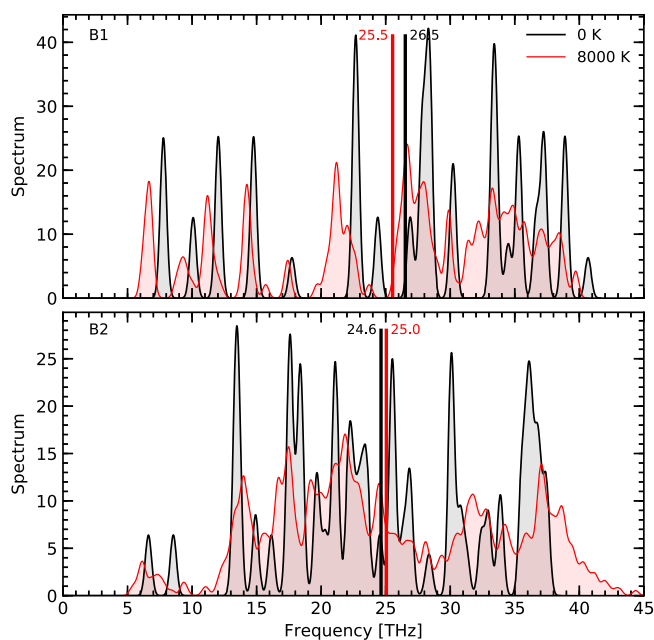

FIG. 2.   Phonon spectrum of the B1 phase at 6.78 (top panel) and the B2 phase at 7.27 g/cm^3 (bottom panel) at 0 and 8000 K. The vertical line shows the average frequency for each spectrum.
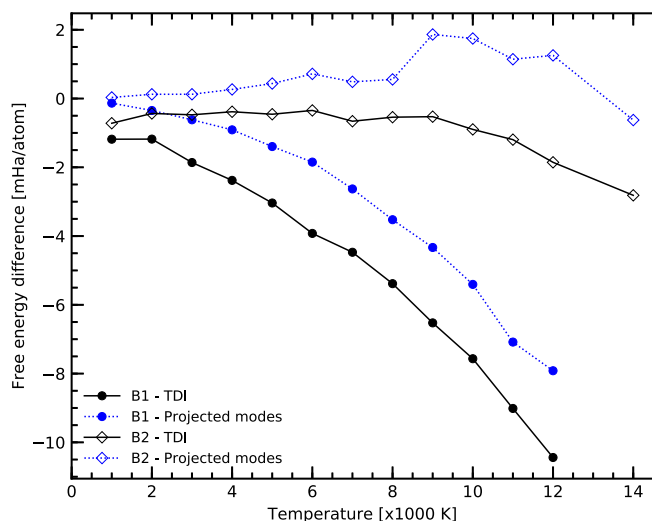
FIG. 3. Helmholtz free energy difference between TDI or PQHA calculations and the QHA predictions for the B1 phase at 6.78 (full circles) and B2 phase at 7.27 g/cm^3 (open diamonds) as a function of the temperature. The full lines show the results of our TDI calculations; the dotted lines stand for our PQHA predictions.
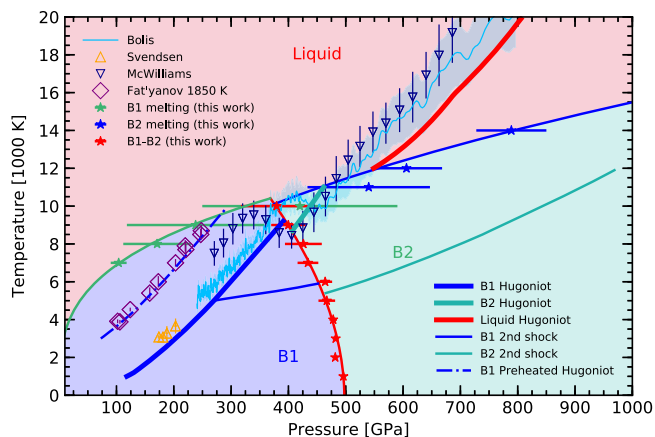

FIG. 4. Comparison of experimental and *ab initio* Hugoniot curves along with the MgO phase diagram as derived with TDI. The thick lines correspond to our Hugoniot calculations for B1 (blue), liquid (red), and B2 (green) phases. We plotted the experimental results of single shocks [13], decaying shocks [26,27], and preheated shocks [28]. We also show our *ab initio* prediction for a double shock Hugoniot curve (thin line) starting from an initial shock that had reached 5000 K, as well as the calculated result for a B1 1850 K preheated Hugoniot (thin dash-dotted line).

calculations in Fig. 3 predict only a slight reduction in the free energy compared to the QHA at high temperature. We can thus conclude that anharmonic effects are marginal in the B2 phase.

The Helmholtz free energy of the B1 phase is much more sensitive to anharmonic effects as we have concluded from the deviations between the predictions from QHA and PQHA already. TDI and PQHA predict free energies that are lower than those obtained with the QHA. This deviation is strongly temperature dependent. This means the higher order terms in the potential decomposition need to be taken into account over the entire temperature range under consideration, not just close to the melting line where one would expect them to be the most important. Except for a simple offset, the TDI calculations in Fig. 3 predict a very similar behavior for the free energy as the PQHA, which explains the agreement with Boates and Bonev [19] since they employed vibrational spectra similarly to the PQHA method. Based on our results, we conclude that QHA cannot capture the exact behavior of the B1 phase as temperature increases.

In Fig. 1 our QHA results retrieve the typical negative shallow slope of the B1-B2 transition that has been reported in the literature [16,18,20–22]. The phonons as computed by QHA favor the B2 phase. Conversely, the TDI results as well as methods including a high level of anharmonicity favor a steep Clapeyron slope. From our TDI and PQHA results, we infer that anharmonic effects stabilize the B1 phase. The difference between the QHA and the TDI at 0 K is due to the inclusion of the zero-point motion in the QHA.

Our B1-B2 transition pressure differs from the recent prediction by Taniuchi *et al.* [22], who provide a single B1-B2 transition point using a different form of TDI. Based on the information provided in their article, we were not able to identify the reasons for the discrepancy.

As shown in Fig. 4, our predictions for the Hugoniot curve in the B1 phase agree well with the single shock experiments [13] at low pressure. At pressures lower than 350 GPa, the calculated B1 Hugoniot is in agreement with Bolis *et al.* decaying shock experiments [27]. For the B1 phase, we also calculated a Hugoniot curve with an initial state that was preheated at 1850 K. We found excellent agreement with the very precise measurements from Fat'yanov *et al.* [28]. The calculated liquid Hugoniot is within the error bars of Bolis *et al.* [27] but slightly lower than McWilliams *et al.* [26]. We also computed the Hugoniot prediction for the B2 phase but it spans a small range of pressures. The predicted Hugoniot somewhat lies close to the experimental measurements. But we notice also that the calculated B2 Hugoniot is relatively close to the B1 Hugoniot because the volume difference is small. Thus, the large discontinuity observed in the experiment cannot be satisfactorily explained by a B1-B2 transition. Based on our phase diagram and Hugoniot curves, for shock experiments that reach thermodynamic equilibrium, we predict, as pressure increases, the Hugoniot curve to pass through the B1 phase, then to briefly exhibit a B2 phase and then to follow the B2 melting line before entering the liquid phase. However, due to the uncertainty on the exact location of the triple point it is possible that

the principal Hugoniot actually goes right on top of the triple point.

It is difficult to predict what happens in shock experiments that do not necessarily reach thermodynamic equilibrium. The direct comparison of computed predictions with the decaying shock experiments thus requires caution. Nevertheless the observed discontinuity is at slightly lower temperature conditions than our B1 or B2 melting line. But experiments as well as *ab initio* simulations have uncertainties. It might be possible in principle to reconcile the experimental and our computational predictions. It is possible that the experimental shock conditions come very close to the triple point and that a mixture of B1, B2, and liquid was generated. This would explain the presence of a single discontinuity. We advocate for the development of shock experiments coupled to high accuracy x-ray measurements and applied to MgO. In Fig. 4, we give an example for a double shock experiment that reaches deeply into the domain of the B2 phase and for which it would be easier to detect the B1-B2 transition with x rays.

Overall, with *ab initio* methods, we computed the phase diagram of MgO from 50 to 2000 GPa and determined the boundaries between B1, B2, and liquid phases. With two methods, TDI and PQHA, we demonstrated that anharmonic effects at elevated temperatures shift the B1-B2 transition to higher pressures. While the QHA is numerically very efficient and convenient, it provides an insufficient description of MgO at elevated temperatures. This suggests that similar trends may also occur for other materials, in particular if anharmonic effects are much larger in one phase than in another.

Because of such effects, we predict that the principal Hugoniot curve of MgO to pass through the B1 phase, then enter briefly the B2 stability region before reaching the melting line and then the liquid phase. But because of the closeness to the triple point, the melting and the formation of the B2 phase may both contribute to the negative dT/dP behavior observed in recent shock experiments.

[1] The Extrasolar Planets Encyclopedia, http://exoplanet.eu/.

[2] W. J. Borucki *et al.*, Science **327**, 977 (2010).

[3] *The CoRoT Mission, Pre-Launch Status, Stellar Seismology and Planet Finding*, edited by M. Fridlund, A. Baglin, J. Lochard, and L. Conroy (European Space Agency, Munich, 2006).

[4] A. E. Ringwood, Geochim. Cosmochim. Acta **55**, 2083 (1991).

[5] D. Valencia, R. J. O'Connell, and D. Sasselov, Icarus **181**, 545 (2006).

[6] L. Stixrude, Phil. Trans. R. Soc. A **372**, 20130076. (2014).

[7] N. Nettelmann, R. Helled, J. J. Fortney, and R. Redmer, Planet. Space Sci. **77**, 143 (2013).

[8] N. Nettelmann, K. Wang, J. J. Fortney, S. Hamel, S. Yellamilli, M. Bethkenhagen, and R. Redmer, Icarus **275**, 107 (2016).

[9] B. Militzer, F. Soubiran, S. M. Wahl, and W. B. Hubbard, J. Geophys. Res. Planets **121**, 1552 (2016).

[10] W. B. Hubbard and B. Militzer, Astrophys. J. **820**, 80 (2016).

[11] S. M. Wahl, W. B. Hubbard, B. Militzer, T. Guillot, Y. Miguel, N. Movshovitz, Y. Kaspi, R. Helled, D. Reese, E. Galanti, S. Levin, J. E. Connerney, and S. J. Bolton, Geophys. Res. Lett. **44**, 4649 (2017).

[12] J. Leconte and G. Chabrier, Astron. Astrophys. **540**, A20 (2012).

[13] B. Svendsen and T. J. Ahrens, Geophys. J. R. Astron. Soc. **91**, 667 (1987).

[14] T. S. Duffy, R. J. Hemley, and H. K. Mao, Phys. Rev. Lett. **74**, 1371 (1995).

[15] F. Coppari, R. F. Smith, J. H. Eggert, J. Wang, J. R. Rygg, a. Lazicki, J. a. Hawreliak, G. W. Collins, and T. S. Duffy, Nat. Geosci. **6**, 926 (2013).

[16] A. R. Oganov, M. J. Gillan, and G. D. Price, J. Chem. Phys. **118**, 10174 (2003).

[17] D. Alfè, M. Alfredsson, J. Brodholt, M. J. Gillan, M. D. Towler, and R. J. Needs, Phys. Rev. B **72**, 014114 (2005).

[18] D. Cebulla and R. Redmer, Phys. Rev. B **89**, 134107 (2014).

[19] B. Boates and S. A. Bonev, Phys. Rev. Lett. **110**, 135504 (2013).

[20] S. Root, L. Shulenburger, R. W. Lemke, D. H. Dolan, T. R. Mattsson, and M. P. Desjarlais, Phys. Rev. Lett. **115**, 198501 (2015).

[21] K. Miyanishi, Y. Tange, N. Ozaki, T. Kimura, T. Sano, Y. Sakawa, T. Tsuchiya, and R. Kodama, Phys. Rev. E **92**, 023103 (2015).

[22] T. Taniuchi and T. Tsuchiya, J. Phys. Condens. Matter **30**, 114003 (2018).

[23] J. Bouchet, F. Bottin, V. Recoules, F. Remus, G. Morard, R. M. Bolis, and A. Benuzzi-Mounaix, Phys. Rev. B **99**, 094113 (2019).

[24] R. Musella, S. Mazevet, and F. Guyot, Phys. Rev. B **99**, 064110 (2019).

[25] A. B. Belonoshko, S. Arapan, R. Martonak, and A. Rosengren, Phys. Rev. B **81**, 054110 (2010).

[26] R. S. Mcwilliams, D. K. Spaulding, J. H. Eggert, P. M. Celliers, D. G. Hicks, R. F. Smith, G. W. Collins, and R. Jeanloz, Science **338**, 1330 (2012).

[27] R. M. Bolis, G. Morard, T. Vinci, A. Ravasio, E. Bambrink, M. Guarguaglini, M. Koenig, R. Musella, F. Remus, J. Bouchet, N. Ozaki, K. Miyanishi, T. Sekine, Y. Sakawa, T. Sano, R. Kodama, F. Guyot, and A. Benuzzi-Mounaix, Geophys. Res. Lett. **43**, 9475 (2016).

[28] O. V. Fat'yanov, P. D. Asimow, and T. J. Ahrens, Phys. Rev. B **97**, 024106 (2018).

[29] G. Kresse and J. Furthmüller, Phys. Rev. B **54**, 11169 (1996).

[30] S. Nosé, J. Chem. Phys. **81**, 511 (1984).

[31] S. Nosé, Prog. Theor. Phys. Suppl. **103**, 1 (1991).

[32] N. D. Mermin, Phys. Rev. **137**, A1441 (1965).

[33] W. Kohn and L. J. Sham, Phys. Rev. **140**, A1133 (1965).

[34] J. P. Perdew, K. Burke, and M. Ernzerhof, Phys. Rev. Lett. **77**, 3865 (1996).

[35] P. E. Blöchl, Phys. Rev. B **50**, 17953 (1994).

[36] G. A. de Wijs, G. Kresse, and M. J. Gillan, Phys. Rev. B **57**, 8223 (1998).

[37] H. F. Wilson and B. Militzer, Phys. Rev. Lett. **104**, 121101 (2010).

[38] H. F. Wilson and B. Militzer, Astrophys. J. **745**, 54 (2012).

[39] H. F. Wilson and B. Militzer, Phys. Rev. Lett. **108**, 111101 (2012).

[40] B. Militzer, Phys. Rev. B **87**, 014202 (2013).

[41] S. M. Wahl, H. F. Wilson, and B. Militzer, Astrophys. J. **773**, 95 (2013).

[42] S. M. Wahl and B. Militzer, Earth Planet. Sci. Lett. **410**, 25 (2015).

[43] F. Soubiran and B. Militzer, Astrophys. J. **806**, 228 (2015).

[44] F. Soubiran and B. Militzer, Astrophys. J. **829**, 14 (2016).

[45] D. Frenkel and B. Smit, *Understanding Molecular Simulation: from Algorithms to Applications* (Academic Press, New York, 2002).

[46] See Supplemental Material at http://link.aps.org/supplemental/10.1103/PhysRevLett.125.175701 for a detailed calculation of the heat capacity in the B1 phase, the absolute Helmholtz free energies corresponding to Fig. 3, and an analysis of the effects of finite size and of the center-of-mass correction on the B1-B2 transition.

[47] G. Navascués and E. Velasco, J. Chem. Phys. **132**, 134106 (2010).

[48] P. Brüesch, *Phonons: Theory and Experiments I*, 1st ed., edited by M. Cardona, P. Fulde, and H.-J. Queisser (Springer, Berlin Heidelberg, 1982).

[49] A. Henry and G. Chen, J. Comput. Theor. Nanosci. **5**, 141 (2008).

[50] M. P. Allen and D. J. Tildesley, *Computer Simulation of Liquids* (Clarendon Press, Oxford, 1987).

[51] D. Alfè, Phys. Rev. Lett. **94**, 235701 (2005).